polymers

MDPI

Article

Preparation and Characterization of Magadiite–Magnetite Nanocomposite with Its Sorption Performance Analyses on Removal of Methylene Blue from Aqueous Solutions

Mingliang Ge [1,2,3], Zhuangzhuang Xi [1], Caiping Zhu [1], Guodong Liang [2], Guoqing Hu [1], Lafifa Jamal [4] and Jahangir Alam S. M. [1,5,*]

1 Key Laboratory of Polymer Processing Engineering of Ministry of Education, National Engineering Research Center of Novel Equipment for Polymer Processing, School of Mechanical & Automotive Engineering, South China University of Technology, Guangzhou 510640, China; gml@scut.edu.cn (M.G.); zhuangzhuangxi32@gmail.com (Z.X.); 2352446558@163.com (C.Z.); gqhu@scut.edu.cn (G.H.)
2 Key Laboratory of Polymeric Composite & Functional Materials of Ministry of Education, Sun Yat-Sen University, Guangzhou 510275, China; lgdong@mail.sysu.edu.cn
3 School of Material Science and Engineering, Guizhou Minzu University, Guiyang 550000, China
4 Department of Robotics & Mechatronics Engineering, University of Dhaka, Dhaka 1000, Bangladesh; lafifa@du.ac.bd
5 Department of Computer Science & Engineering, Jessore University of Science and Technology, Jessore 7408, Bangladesh
* Correspondence: mejahangir@scut.edu.cn; Tel.: +86-132-502-54060 or +86-135-339-19779

Received: 16 February 2019; Accepted: 25 March 2019; Published: 2 April 2019

Abstract: The magadiite–magnetite (MAG–Fe_3O_4) nanocomposite has great potential applications in the field of biomaterials research. It has been used as a novel magnetic sorbent, prepared by co-precipitation method. It has the dual advantage of having the magnetism of Fe_3O_4 and the high adsorption capacity of pure magadiite (MAG). MAG–Fe_3O_4 was characterized by X-ray diffraction (XRD), Fourier transform infrared spectroscopy (FTIR), scanning electron microscopy (SEM), and vibrating sample magnetometer (VSM). The results showed that Fe_3O_4 nanoparticles were deposited on the interlayer and surface of magadiite. MAG–Fe_3O_4 was treated as an adsorbent for methylene blue (MB) removal from aqueous solutions. The adsorption properties of MAG–Fe_3O_4 were investigated on methylene blue; however, the results showed that the adsorption performance of MAG–Fe_3O_4 improved remarkably compared with MA and Fe_3O_4. The adsorption capacity of MAG–Fe_3O_4 and the removal ratio of methylene blue were 93.7 mg/g and 96.2%, respectively (at 25 °C for 60 min, pH = 7, methylene blue solution of 100 mg/L, and the adsorbent dosage 1 g/L). In this research, the adsorption experimental data were fitted and well described using a pseudo-second-order kinetic model and a Langmuir adsorption isotherm model. The research results further showed that the adsorption performance of MAG–Fe_3O_4 was better than that of MAG and Fe_3O_4. Moreover, the adsorption behavior of MB on MAG–Fe_3O_4 was investigated to fit well in the pseudo-second-order kinetic model with the adsorption kinetics. The authors also concluded that the isothermal adsorption was followed by the Langmuir adsorption isotherm model; however, it was found that the adsorption of the MAG–Fe_3O_4 nanocomposite was a monolayer adsorption.

Keywords: magnetic; nanocomposite; Fe_3O_4; magadiite; adsorption; methylene blue

1. Introduction

Water pollution is seriously damaging the environment as well as threatening human existence and development. According to reports, a large number of poisonous and harmful contaminants (e.g., heavy metal ions, nitrite, and organic dyes) were directly poured into natural water bodies [1]. Wastewater with organic dyes is especially toxic and non-biodegradable; dyes are difficultly treated, and, even at low concentration, are harmful to human beings and microorganisms [2,3]. Accordingly, the technologies to treat dye wastewater has attracted more attention, and multiple technologies were developed for remove organic dyes pollutant from various aqueous solutions [4]. Until now, the conventional methods of treating wastewater has included chemical precipitation, adsorption, filtration, and ion exchange [5–8]. Moreover, the adsorption method has been proven to be one of the favored techniques, owing to its convenience and effectiveness [9–12]. The common adsorbents, including activated carbon, cellulosic biomass [13], as well as—according to the latest reports—chitosan [14,15] and silicate materials [16–18] has a low cost but also excellent adsorption properties.

Magadiite (MAG) is a kind of layered silicate material [19,20] that possesses a large amount of potentially exchangeable hydrated sodium ions between its layers [21]; for this reason, MAG has unique properties, such as high surface area, good ion exchange, and expansion [22,23]. MAG showed excellent adsorption performance on heavy metal ions and organic pollutants [24–26], although it was difficult to separate from the water after adsorption. Fe_3O_4 is a typical superparamagnetic nanoparticle with chemical stability, large specific surface area, easy separation, and good biocompatibility [27–30], but it is also easy to agglomerate in the aqueous system to influence on its adsorption properties because of its small particle size [31]. Therefore, it has a conceivable capability as a magnetic composite, which loaded the magnetite on MAG to solve the problems of separation of MAG and the aggregation of magnetite (Fe_3O_4) in the aqueous solutions.

Until now, the Fe_3O_4 nano-composite has been prepared using the co-precipitation method, and the composite exhibits high adsorption ability for dyes, while the magnetic separation effect is remarkable [32]; it was reported that Fe_3O_4–montmorillonite nanocomposite, showing good stability and reusability, was synthesized using the co-precipitation method [33] and exhibited excellent adsorption properties for Pb^{2+}, Cu^{2+}, and Ni^{2+} [34]. In this research, the MAG–Fe_3O_4 nanocomposite was prepared using a co-precipitation method, with Fe_3O_4 nanoparticles deposited on the interlayer and surface of MAG. Methylene blue (MB) was chosen as a model organic dye to investigate the adsorption properties of the MAG–Fe_3O_4 nanocomposite.

2. Experimental

2.1. Materials Collection

Anhydrous ferric chloride ($FeCl_3$) (chemical pure) was purchased from Sinopharm Chemical Reagent Co., Ltd., Beijing, China. Ferrous chloride ($FeCl_2{\cdot}4H_2O$) (analytical pure), Hydrochloric acid (HCl) (analytical pure), and Methylene blue (MB) (analytical pure) were obtained from Guangzhou Chemical Reagent Factory, Guangzhou, China. Sodium hydroxide (NaOH) (analytical pure) was provided by Tianjin Chemical Reagent Factory, Tianjin, China, and South China University of Technology, Guangzhou, China.

2.2. Preparation of MAG-Fe_3O_4

MAG was prepared in the laboratory according to reference [35]. The MAG–Fe_3O_4 nanocomposite was prepared by co-precipitation method. A dose of 2.32 g MAG was dispersed in 50 mL deionized water, sonicated for 10 min, then stirred for 12 h by mechanical agitator to obtain the MAG dispersion solution. The iron salts, 0.04 mol $FeCl_2{\cdot}4H_2O$ and 0.03 mol $FeCl_3$, were added to a three-mouth flask containing 50 mL deionized water under the presence of N_2 gas, stirred by a mechanical agitator to obtain the solution of Fe^{2+} and Fe^{3+} ($n(Fe^{2+}):n(Fe^{3+}) = 4:3$). Then, the MAG dispersion solution was added to the solution of Fe^{2+} and Fe^{3+} under vigorous stirring and stable N_2 flow, the Fe^{2+} and Fe^{3+}

enter the interlayer of MAG by ion exchange with the Na^+ between the layers of MAG. Afterward, the 20 mL of 0.4 mol/L NaOH solution was added dropwise to the mixture solution, the Fe^{2+} and Fe^{3+} reacted with OH^- to form Fe_3O_4, and attached to the inside and outside of the layer of MAG; the chemical reaction equation is $Fe^{2+} + 2Fe^{3+} + 8OH^- = Fe_3O_4 + 4H_2O$. The reaction solution was kept at 80 °C for 2 h in the presence of an N_2 gas. The precipitate was separated by a permanent magnet, washed with absolute ethanol for three times, and dried at 80 °C for 24 h in a vacuum to obtain MAG–Fe_3O_4 nanocomposites.

2.3. Instruments

In order to evaluate the adsorbents and adsorption products, X-ray diffraction (XRD) analyses patterns on the samples were performed using an AXS D8 ADVANCE X-ray diffractometer (Bruker, Karlsruhe, Germany) with Cu-Kα radiation operated at 40 kV and 40 mA. Fourier transform infrared spectroscopy (FTIR) was used to record and investigate the structure of constituents as well as chemical changes in materials in the range of 400~4000 cm^{-1} by NEXUS 670 type FTIR (Nicolet, Waltham, MA, USA). A scanning electron microscope (SEM) was used to observe the surface morphology of the adsorbent samples by LEO 1530VP type SEM (Zeiss, Oberkochen, Germany). A vibrating sample magnetometer (VSM) was used to measure the magnetic characterization of the material by the VSM 7404 type VSM (Lakeshore, Columbus, OH, USA) at 298 K with magnetic fields up to 8000 Oe.

2.4. Characterization Study

2.4.1. Batch Adsorption Experiments

In order to analyze the adsorption performance of MAG–Fe_3O_4, batch adsorption experiments were performed to investigate the effects of influential parameters, such as solution pH, adsorbent dose, contact time, and concentration. To perform the adsorption experiments, 50 mL MB solutions with different concentrations (30, 50, 80, 100, 120, and 150 mg/L) were carried out individually in 150 mL glass bottles. The adsorption experiments were conducted at room temperature (25 °C) and the pH values were kept at 7. Different amounts of MAG–Fe_3O_4 nanocomposites (12.5, 25, 37.5, 50, 62.5 and 75 mg) were added into the MB solution, the mixture solutions were stirred at 25 °C with the contact time between 5 and 120 min, and the adsorbents (MAG-Fe_3O_4 nanocomposite) were separated from the solution by the magnetic separation technique (MST). The concentrations of MB in the supernatants were measured at 664 nm with 53WUV/VIS type ultraviolet-visible spectrophotometer (UVS) (produced by Shanghai Analytical Instrument Factory, China). The results of the removal rate were found to express as the removal efficiency (%) of the adsorbent toward MB, which was defined as:

$$\text{Removal efficiency, } \eta(\%) = \left(\frac{C_0 - C_t}{C_0}\right) \times 100\% \quad (1)$$

where C_0 is the initial concentrations (mg/L) of adsorbates (MB), and C_t is the concentration of adsorbates (MB) at time t in the adsorbents (MAG-Fe_3O_4 nanocomposite) solution (mg/L).

The adsorption capacity of MB is the concentration of MB on the adsorbent mass, and it was calculated based on the mass balance principle:

$$\text{Adsorption capacity, } q_t\ (\text{mg/g}) = \frac{(C_0 - C_t) \times V}{m} \quad (2)$$

where q_t is the adsorbing capacity of adsorbents (MAG–Fe_3O_4 nanocomposite) (mg/g), C_t is the adsorbates (MB) concentration at time t in the adsorbents (MAG–Fe_3O_4 nanocomposite) solution (mg/L), V is the volume of the adsorption adsorbates (MB) solution (mL), and m is the mass of the adsorbents (MAG–Fe_3O_4 nanocomposite) in the solution (g).

2.4.2. Adsorption Kinetics Study

The adsorption kinetics is the study of the influence of various factors on the adsorption rate, careful monitoring of the experimental conditions which influence the speed of a chemical reaction and helps to obtain the equilibrium in a reasonable length of time. The adsorption kinetics of solutes in a solution by solid adsorbents is described by the pseudo-first-order and pseudo-second-order kinetic models [36,37].

Pseudo-First-Order Kinetic Model

The pseudo-first-order kinetic model is the adsorption kinetic equation which was applied to the liquid phase. The pseudo-first-order kinetic equation can be expressed as the following:

$$\ln(q_{eq} - q_t) = \ln q_{eq} - K_1 t \tag{3}$$

where q_{eq} is the amount of adsorption (mg/g) at equilibrium, q_t is the amount of adsorption (mg/g) at time t, and K_1 is the rate constant (min^{-1}) of the pseudo-first-order kinetic equation (g/mg min).

Pseudo-Second-Order Kinetic Model

The pseudo-second-order kinetic model was assumed that the adsorption process was controlled by the chemisorption mechanism. The pseudo-second-order kinetic equation can be expressed as in the following:

$$\frac{t}{q_t} = \frac{1}{K_2 q_{eq}^2} + \frac{t}{q_{eq}} \tag{4}$$

where q_{eq} is the amount of adsorption (mg/g) at equilibrium, q_t is the amount of adsorption (mg/g) at time t, and K_2 (g/mg min) is the rate constant of the pseudo-second-order kinetic equation.

2.4.3. Adsorption Isotherms

The adsorption isotherm is a curve which shows the relationship between the adsorption capacity and the initial concentration of the solution under certain temperature conditions. The effects of the adsorbent and the adsorbate can be judged by the variation of the adsorption isotherm. The commonly used adsorption isotherm models were introduced as Langmuir and Freundlich models [38]. In this study, the adsorption isotherm data were analyzed with the classical Langmuir isotherm model and Freundlich isotherm models.

Langmuir Isotherm Model

The Langmuir model, based on the adsorption kinetics and conforming to the monolayer adsorption mechanism, is deduced by a series of hypotheses and can be used to calculate the maximum adsorption capacity q_m (the theoretical saturated adsorption capacity). To ensure the equilibrium conditions, the linear form of the Langmuir isotherm model was applied to the experimental data. The Langmuir isotherm equation is given as in the following:

$$\frac{c_{eq}}{q_{eq}} = \frac{1}{K_L q_m} + \frac{c_{eq}}{q_m} \tag{5}$$

$$R_L = \frac{1}{K_L q_m + c_0} \tag{6}$$

where c_0 (mg/L) is the initial concentration of MB solution, c_{eq} (mg/L) is the concentration of MB solution at equilibrium, q_{eq} (mg/g) is the adsorption capacity at equilibrium, q_m (mg/g) is the maximum adsorption capacity of Langmuir adsorption model, R_L is the adsorption strength, and K_L is the adsorption constants.

Freundlich Isotherm Model

The Freundlich model is a rough estimate of the affinity between adsorbent (MAG–Fe_3O_4 nanocomposite) and adsorbates (MB). The Freundlich isotherm equation can be expressed as in the following:

$$q_{eq} = K_F C_{eq}^{\frac{1}{n}} \quad (7)$$

$$\ln q_{eq} = \frac{1}{n} \ln c_{eq} + \ln K_F \quad (8)$$

where c_{eq} (mg/L) is the concentration of the MB solution at equilibrium, q_{eq} (mg/g) is the adsorption amount unit at equilibrium, $1/n$ and K_F are Freundlich constants that are related to adsorption intensity. The value of n is an indication of the favorability of adsorption (n is called as the characteristic constant).

3. Results and Discussion

3.1. Characterization and Structure Analysis of MAG–Fe_3O_4

3.1.1. XRD Analyses

The XRD patterns of MAG, Fe_3O_4, and MAG–Fe_3O_4 are shown in Figure 1. According to Figure 1a, it was clearly that the characteristic diffraction reflections of MAG appeared at 2θ = 5.58°, 11.32°, 25.64°, 26.76°, 28.18°, and 49.57° [39]. From Figure 1b, the characteristic diffraction reflections of Fe_3O_4 appeared at 2θ = 30.04°, 35.49°, 43.09°, and 57.16° [40–42]. However, according to Figure 1c, the characteristic diffraction reflections of MAG–Fe_3O_4 appeared at 2θ = 5.58°, 11.32°, 25.64°, 26.76°, 28.18°, 49.57°; and at 2θ = 30.04°, 35.49°, 43.09°, 57.16°. The XRD patterns of MAG–Fe_3O_4 has contained both characteristic reflections of MAG and Fe_3O_4, indicating that the MAG–Fe_3O_4 nanocomposite was successfully synthesized by co-precipitation method.

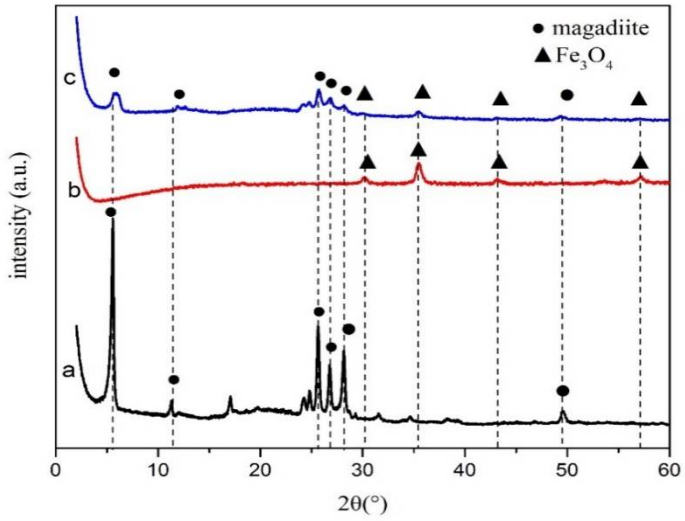

Figure 1. XRD patterns of (**a**) MAG, (**b**) Fe_3O_4, and (**c**) MAG–Fe_3O_4.

3.1.2. FTIR Analyses

The FTIR spectrum of MAG, Fe_3O_4, and MAG–Fe_3O_4 are shown in Figure 2. The FTIR spectroscopy was used to identify the chemical groups of MAG, Fe_3O_4, and MAG–Fe_3O_4. From the FTIR spectrum of MAG and Fe_3O_4, the sorption reflection around the wave number at 3430 cm^{-1} and 1613 cm^{-1} were attributed to the stretching and bending vibration of the O–H bond on the surfaces of MAG and Fe_3O_4. It was found that the reflection band of sorption around the wave number at 1079 cm^{-1} was seen due to the symmetric stretching vibration of the [SiO_4] tetrahedron in MAG [43], whereas the wave number at 785 cm^{-1} and 619 cm^{-1} was assigned to the double rings vibrations in

MAG [43]. However, the wave number at 576 cm^{-1} had corresponded to the stretching vibration of Fe–O in Fe_3O_4 [44–46]. Therefore, the reflection band of sorption around the wave number at 462 cm^{-1} was seen from the flexural vibration of Si–O–Si in MAG. It also showed that the basic skeleton of MAG did not change during the preparation of MAG–Fe_3O_4. The reason why the Fe_3O_4 particles could be loaded on the MAG by electrostatic attraction to reduce their surface energy was that there was a high surface energy of Fe_3O_4 nanoparticles and an intrinsic charge for MAG [47].

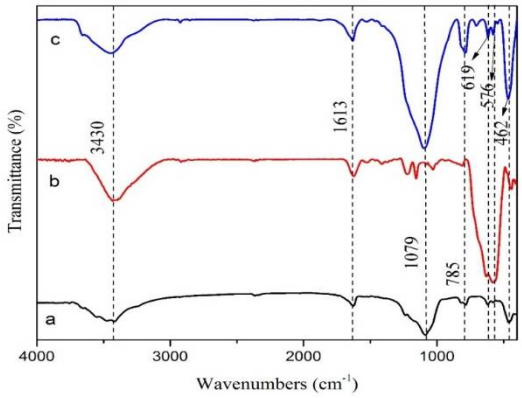

Figure 2. FTIR patterns of (**a**) MAG, (**b**) Fe_3O_4, and (**c**) MAG–Fe_3O_4.

3.1.3. SEM Images Analyses

The SEM images of MAG and MAG–Fe_3O_4 are shown in Figure 3. Figure 3a shows that the MAG was rose-patterned and petal-shaped with a smooth surface. Figure 3b shows that many nanoscale spherical Fe_3O_4 particles adhered on the interlayer and surface of MAG, which indicated that the MAG–Fe_3O_4 nanocomposites were successfully synthesized.

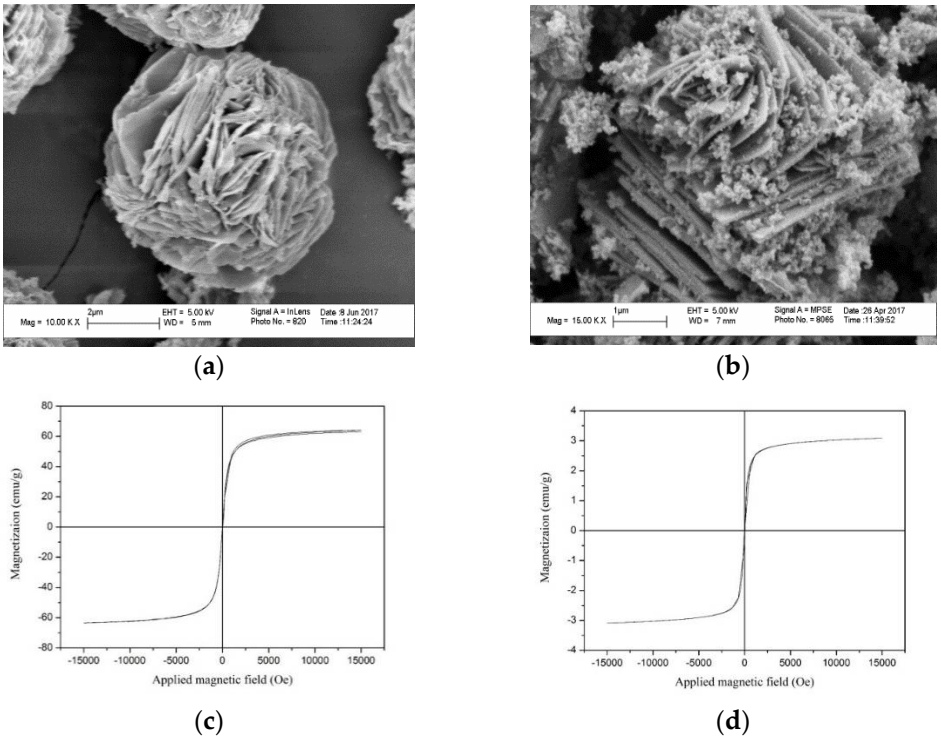

Figure 3. SEM images of (**a**) MAG [48], and (**b**) MAG–Fe_3O_4; and hysteresis loops of (**c**) Fe_3O_4, and (**d**) MAG–Fe_3O_4.

3.1.4. Magnetism Analyses

In order to investigate the magnetic properties of Fe_3O_4 and MAG–Fe_3O_4, the hysteresis loops were tested by VSM. It can be seen from Figure 3c,d that the saturation magnetization of Fe_3O_4 and MAG–Fe_3O_4 were 64.25 emu/g and 3.09 emu/g, respectively. It was found that the MAG–Fe_3O_4 had a certain magnetization as well as the hysteresis loop of the MAG–Fe_3O_4 had passed through the origin, indicating that the MAG–Fe_3O_4 had no remanence and coercively, and it was a typical paramagnetic material [47]. The dispersion of MAG–Fe_3O_4 in deionized water before the action of an applied magnetic field are shown in Figure 4a,b respectively. Without applying the external magnetic field, the MAG–Fe_3O_4 was dispersed uniformly in deionized water, but the solution was muddy, as shown in Figure 4a. By applying the external magnetic field, the MAG–Fe_3O_4 moved to the side of the magnetic field in the solution, and the solution became clarified. As shown in Figure 4b, MAG–Fe_3O_4 was separated easily from the aqueous solution with the magnetic field. In fact, the magnetic separation technology obviously improved the solid–liquid separation and avoided secondary pollution.

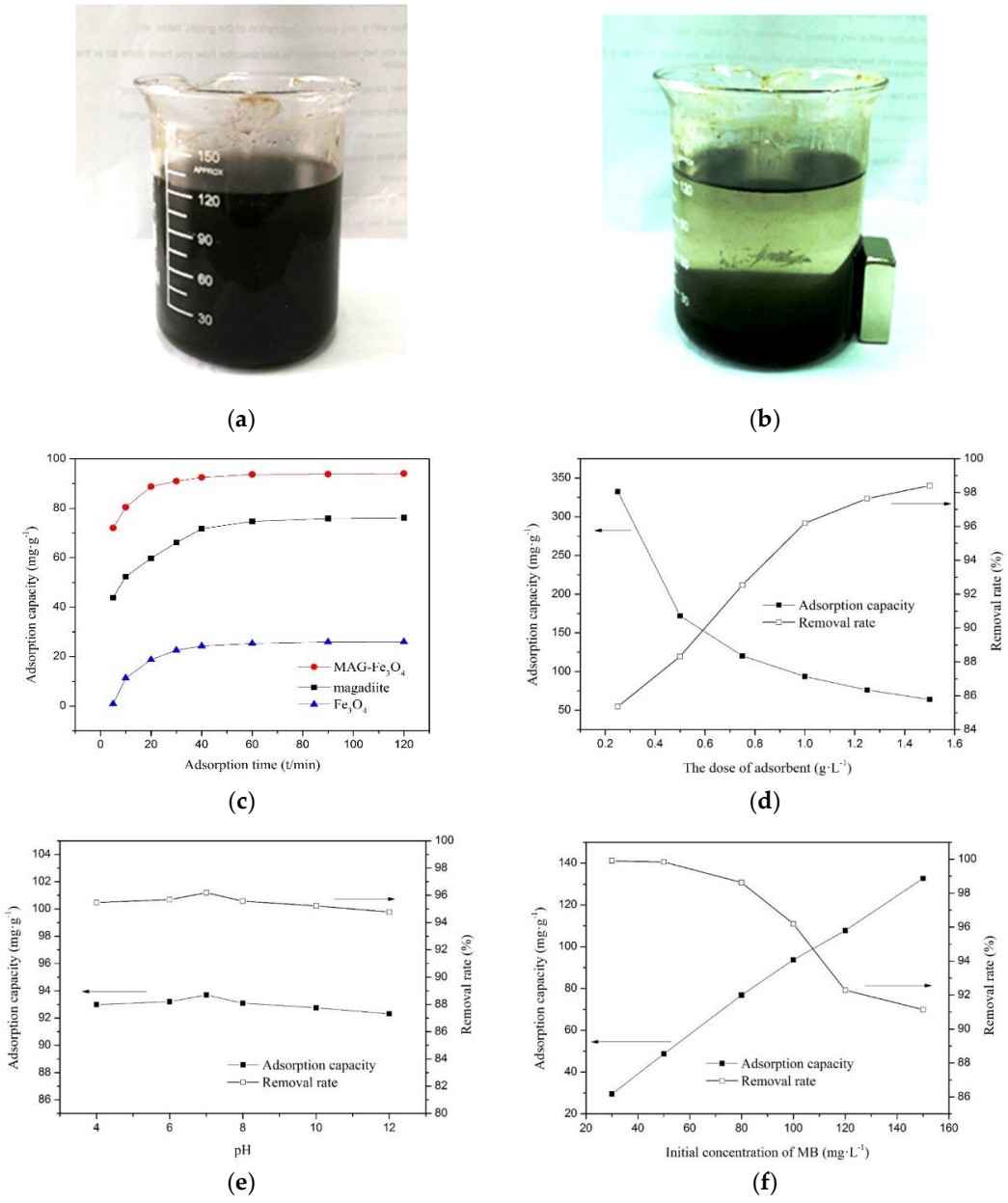

Figure 4. *Cont.*

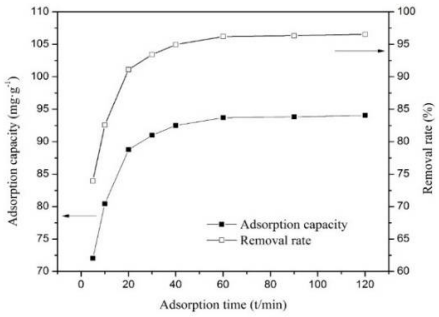

(**g**)

Figure 4. Dispersion of composite MAG–Fe_3O_4 in deionized water: (**a**) before the action of the magnetic field, and (**b**) after the action of the magnetic field; (**c**) Adsorption capacity of MAG, Fe_3O_4, and MAG–Fe_3O_4 (At 25 °C, pH = 7, 100 mg/L MB solution, 1.0 g/L MAG–Fe_3O_4); and effects of (**d**) MAG–Fe_3O_4 dosage on adsorption capacity and removal rate, (**e**) pH on adsorption capacity and removal rate, (**f**) initial concentration of MB on adsorption capacity and removal rate, (**g**) adsorption time on adsorption capacity and removal rate.

3.2. Adsorption Properties of MB on MAG–Fe_3O_4

3.2.1. Adsorption Capacity Analyses of MAG, Fe_3O_4, and MAG–Fe_3O_4

The adsorption capacity of MAG, Fe_3O_4, and MAG–Fe_3O_4 (at 25 °C, pH = 7, 100 mg/L MB solution, 1.0 g/L MAG-Fe_3O_4) are shown in Figure 4c. The adsorption capacity of MAG, Fe_3O_4, and MAG–Fe_3O_4 were measured in order to compare the adsorption properties of MB, as shown in Figure 4c. The equilibrium adsorption capacity of MAG–Fe_3O_4 (94 mg/g) was much higher than the MAG (74.7 mg/g) and the Fe_3O_4 (25.3 mg/g). The adsorption capacity of MAG–Fe_3O_4 increased by about 26% compared with MAG alone, and therefore possessed excellent adsorption properties for MB. This phenomenon was attributed to the fact that Fe_3O_4 inserted itself into the interlays of MAG, and the agglomeration of Fe_3O_4 was inhibited, meaning that more and more active sites of MAG–Fe_3O_4 could be provided than that of MAG and Fe_3O_4. Consecutively, a large number of negative charges on the surfaces of MAG–Fe_3O_4 could contribute to the binding of cationic dye MB [49].

3.2.2. Effect of Adsorbent Dosage on the Adsorption

Adsorbent dosage plays an important role in the adsorption process, because it determines the capacity of an adsorbent for a given initial concentration of the adsorbate. The experiments were carried out in a 100 mg/L MB solution at a temperature of 25 °C, and the pH value of solutions for the adsorption was kept at 7 for 60 min; however, the experiments were carried out at different concentrations of adsorbent MAG–Fe_3O_4 (0.25, 0.5, 0.75, 1, 1.25, and 1.5 g/L).

The influences of the adsorbent dosage on the adsorption performance were the adsorption capacity and removal rate, shown in Figure 4d. The removal rate of MB increased with the increasing of adsorbent dosage; however, the adsorption capacity decreased with increasing adsorbent dosage. On the one hand, with the increasing of the adsorbent dose, the adsorption active sites of the adsorbent also increased and could be adsorbed more MB, and then the removal rate of MB became higher. On the other hand, with the increasing of the adsorbent dose, the adsorption capacity of MAG–Fe_3O_4 decreased, but when the adsorbent solution was 1 g/L, the adsorption capacity of MAG–Fe_3O_4 was 93.7 mg/g, and the removal rate of MB was 96.2%.

Not only was the MAG–Fe_3O_4 tested for its magnetic separation ability, it was also important that the adsorption capacity and removal rate were reached, at 93.7 mg/g and 96.2%, respectively; this was done at 25 °C for 60 min, pH = 7, methylene blue solution of 100 mg/L, and the adsorbent dosage of 1 g/L. Thus, MAG–Fe_3O_4 was proven to be an effective adsorbent.

The definition of adsorption capacity was stated in Equation (2); it decreased in the adsorption capacity though it did not decrease in the amount of adsorption, because the total amount of MB in the solution was constant with the increasing of the dosage of MAG–Fe_3O_4 but the adsorption capacity was gradually decreased. By increasing the dosage of MAG–Fe_3O_4, the removal rate increased but the removal rate of MAG–Fe_3O_4 was more than 85% when the dosage of MAG–Fe_3O_4 was 0.25 g/L; however, it was impossible to reach a removal rate of 100%, due to the dynamic equilibrium of adsorption and desorption. Thus, the solid phase increased by 5, but the removal rate increased by only 10%.

3.2.3. Effect of the Solution pH on Adsorption

The initial pH played an important role in the surface binding sites of the adsorbents and the whole adsorption process. Figure 4e showed the removal rate of MB and the adsorption capacity of MAG–Fe_3O_4 at pH ranges from 4 to 12 at room temperature for 60 min, 100 mg/L of MB solution, and 1 g/L of MAG–Fe_3O_4. It was proven that the adsorption performance of MAG–Fe_3O_4 was affected slightly by pH values; the removal rate was between 94.8% and 96.2%.

3.2.4. Effect of Initial Concentration of MB Solutions on the Adsorption

The effect of the initial concentration of MB was studied and the results were shown in Figure 4f. To investigate the effect of the initial concentration of MB solutions on the adsorption performance, several tests were carried out at 30, 50, 80, 100, 120, and 150 mg/L. As it can be seen from Figure 4f, the initial concentration of MB was significantly affected by the adsorption capacity and removal rate. The adsorption capacity increased quickly with the increasing initial concentration of MB as well as the decreasing removal rate. In addition, when the concentration of the MB solution was low, the active sites of MAG–Fe_3O_4 were sufficient in the solution; however, the MB was almost completely adsorbed by MAG–Fe_3O_4.

3.2.5. Effect of Contact Time on the Adsorption

Equilibrium time is one of the most important parameters in the design of economical adsorption treatment system. Figure 4g shows the effect of contact time on the adsorption of MB on MAG–Fe_3O_4 at temperature 25 °C, the pH value of 7, the concentration of 100 mg/L MB solution, and the amount of 1 g/L MAG–Fe_3O_4. Figure 4g shows that the adsorption capacity and removal rate increased rapidly during the first 20 min, then the adsorption capacity increased slowly as prolonged contact time, after 60 min, the adsorption equilibrium was reached finally. This fact had also reported by other researchers [50–55].

3.2.6. Adsorption Kinetics Analyses

In order to evaluate the adsorption, the kinetic of MB on MAG–Fe_3O_4, the pseudo-first-order and pseudo-second-order adsorption kinetics model equations were adopted to fit the experimental data. The simulated curves of the kinetic equation for the MB adsorption on MAG–Fe_3O_4 are shown in Figure 5a,b and, the related fitting parameters of the pseudo-first-order model and the pseudo-second-order model are listed in Table 1 (q_{eq}—Adsorption capacity of adsorption equilibrium by experiment; q_{eqc}—Adsorption capacity of adsorption equilibrium by calculation; K—Adsorption rate constants; and R^2—Correlation coefficient). It was clearly shown that the correlation coefficient (R^2 = 0.99996) of the pseudo-second-order kinetic model was much closer to 1 than the correlation coefficient (R^2 = 0.94821) of the pseudo-first-order kinetic model. In addition, the equilibrium adsorption capacity q_{eqc} was calculated from the pseudo-second-order, which was closer to the experimental value. Therefore, the pseudo-second-order model was more suitable to describe the adsorption process which was indicated that the reaction rate was linear of the concentration of the two reactants (MAG–Fe_3O_4 and MB). The most important fact is that it was used to calculate the reaction rate constant (K_2 = 0.00689) of the pseudo-second-order model, which intuitively showed the speed of adsorption rate in

adsorption mechanism of the MB removal. The faster adsorption rate was found while the larger value of reaction rate constant (K_2) was performed, whereas the required time for the adsorption calculation was accounted according to the reaction rate constant (K_2).

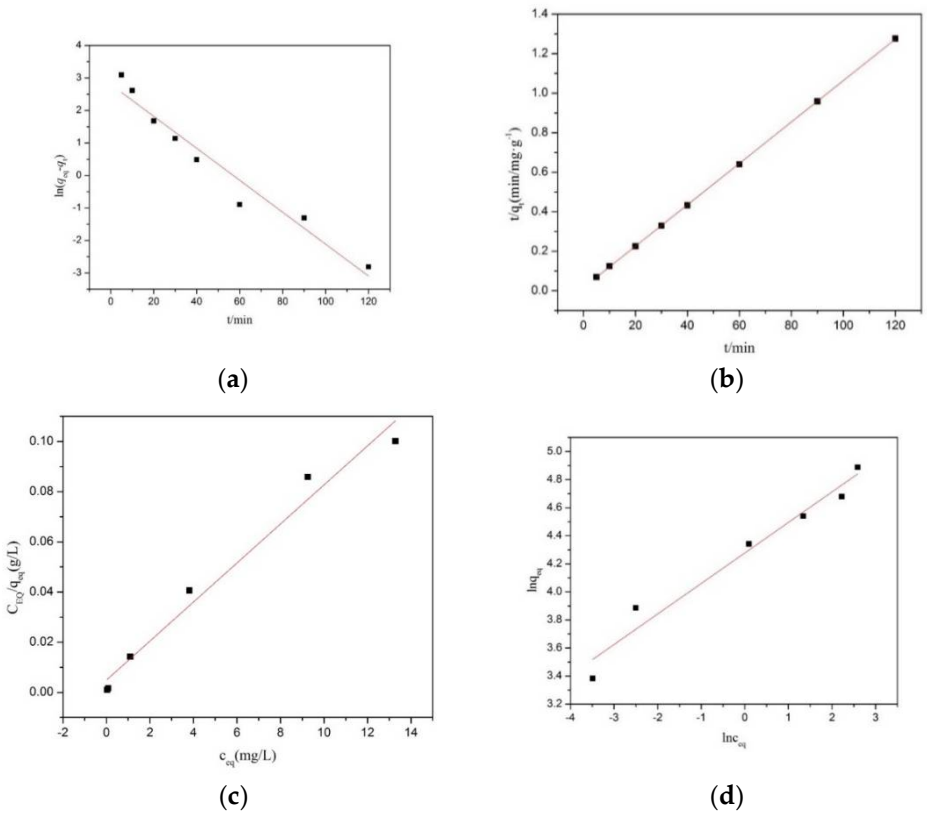

Figure 5. Simulated curves of kinetic equation for MB adsorption on MAG–Fe_3O_4: (**a**) pseudo-first-order model, and (**b**) pseudo-second-order model; and fitted adsorption isotherm models: (**c**) Langmuir model for adsorption of MB on MAG–Fe_3O_4, and (**d**) Freundlich model for adsorption of MB on MAG–Fe_3O_4.

Table 1. Fitting parameters of adsorption kinetic equations.

Model	q_{eq} (mg/g)	q_{eqC} (mg/g)	K	R^2
Pseudo-first-order	94.1	16.4976	0.04915	0.94821
Pseudo-second-order	94.1	95.4198	0.00689	0.99996

3.2.7. Adsorption Isotherm Analyses

In order to study the interactive behavior between MAG–Fe_3O_4 and MB, the Langmuir and Freundlich adsorption isothermal models were employed to simulate the process of adsorption. The linear fitting result of the adsorption isotherms of MAG–Fe_3O_4 was presented in Figure 5c,d, whereas the fitting parameters and regression coefficients (R^2) of isothermal models were tabulated in Table 2. As seen from Table 2, the correlation coefficients of the Langmuir model (R^2 = 0.971) was better than the Freundlich model (R^2 = 0.95725). Furthermore, the maximum adsorption capacity of the Langmuir model was 128.5 mg/g, which was closed to the experimental value of 132.7 mg/g. The concluding remarks can be referenced from another research report that the adsorption process of MB on MAG–Fe_3O_4 was consistent with monolayer adsorption [33]. It was also reported that the adsorption intensity of the Langmuir model could be expressed by R_L, when $0 < R_L < 1$, indicating favorable adsorption [56,57]. Therefore, in this research experiment, the initial concentration of c_0 was

fitted between 30 mg/L and 150 mg/L as well as the regression coefficients were considered as R_L = 0.0028~0.0043, which embodied a favorable adsorption.

Table 2. Fitting parameters of adsorption isotherm models.

Langmuir Model			Freundlich Model		
q_m (mg/g)	K_L (L/mg)	R^2	n		R^2
128.5347	1.591	0.971	4.6	72.057	0.95725

MAG–Fe_3O_4 was generated by treating the adsorbed MAG–Fe_3O_4 with ethanol, then the removal rate of the regenerated MAG–Fe_3O_4 was measured, and the whole process was repeated five times to acquire excellent results. Figure 6 shows that the removal rate of MB by MAG–Fe_3O_4 was over 82.84% after five times, indicating that MAG–Fe_3O_4 has perfect reusability.

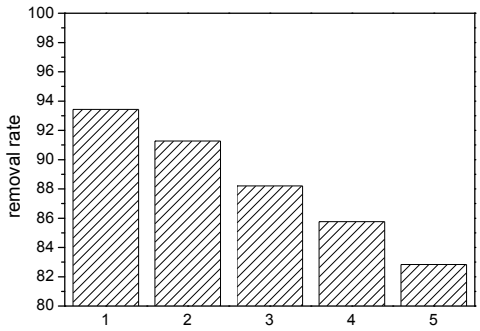

Figure 6. Recycling of MAG-Fe_3O_4

The concentration of 100 mg/L MB solution and 1 g/L MAG-Fe_3O_4 were stirred at 25 °C for 60 min at a pH value of 7; the adsorption capacity of MAG–Fe_3O_4 was 93.7 mg/g while the adsorption capacity of MAG was 74.7 mg/g, the rice biomass was 8.13 mg/g [58], synthetic nano-clay magadiite (SNCM) was 20.00 mg/g [59], Zeolite was 41.26 mg/g [60], TiO_2 was 57.14 mg/g [61], and montmorillonite (MMT) was 64.43 mg/g, as shown in Table 3. The results indicate that MAG–Fe_3O_4 is an efficient low-cost adsorbent.

Table 3. Comparison of MB adsorption capacity with other reported systems.

Adsorbents	Adsorption Capacity (mg/g)	References
Rice biomass	8.13 mg/g	[58]
SNCM	20.00 mg/g	[59]
Zeolite	41.26 mg/g	[60]
TiO_2	57.14 mg/g	[61]
MMT	64.43 mg/g	[33]
MAG	74.7 mg/g	This work
MAG-Fe_3O_4	93.7 mg/g	This work

4. Conclusions

It can be concluded that the MAG–Fe_3O_4 nanocomposite was successfully prepared using the co-precipitation method, and further applied to adsorb cationic organic dye MB from aqueous solutions. The magnetic nanoparticles Fe_3O_4 were deposited on the interlayer and surface of MAG. The morphology, as well as structural properties of MAG–Fe_3O_4, was characterized by XRD, FTIR, SEM, and VSM. The concentration of 100 mg/L MB solution and 1 g/L MAG–Fe_3O_4 were stirred at a temperature of 25 °C for 60 min with a pH value of 7; the adsorption capacity of MAG–Fe_3O_4 and the removal ratio of methylene blue were found as 93.7 mg/g and 96.2%, respectively. The research

results showed that the adsorption performance of MAG–Fe_3O_4 was better than that of MAG and Fe_3O_4. The adsorptions behaviors of MB on MAG–Fe_3O_4 were investigated to fit well in the pseudo-second-order kinetic model with the adsorption kinetics. However, it can be concluded that the isothermal adsorption was followed by the Langmuir adsorption isotherm model, which found and illustrated that the adsorption of MAG–Fe_3O_4 nanocomposite was a monolayer adsorption.

Author Contributions: Conceptualization, M.G.; Data curation, C.Z., Z.X., and J.A.S.M.; Formal analysis, C.Z., Z.X., and J.A.S.M.; Funding acquisition, M.G., G.L., and G.H.; Investigation, M.G. and G.L.; Methodology, C.Z., Z.X., and G.L.; Project administration, M.G., G.L., and G.H.; Resources, M.G., G.L., and G.H.; Software, J.A.S.M. and L.J.; Supervision, M.G.; Validation, G.L.; Visualization, J.A.S.M. and L.J.; Writing—original draft, C.Z.; Writing—review & editing, J.A.S.M.

Funding: The authors gratefully acknowledge the financial support of this research work by the Natural Science Foundation of Guangdong Province Project (Project No. 2016A030313520), Key Laboratory of Polymeric Composite & Functional Materials of Ministry of Education Project (Project No. PCFM-2017-02), Guangdong Water Conservancy Science and Technology Innovation Project (Project No. 2017-24), and Guangdong Provincial Department of Education Featured Innovation Project (Project No. 2017KTSCX007).

Acknowledgments: The authors are grateful to the reviewers for their valuable comments that helped to enrich the publication.

Conflicts of Interest: The authors declare no conflict of interest. The funders had no role in the design of the study; in the collection, analyses, or interpretation of data; in the writing of the manuscript, and in the decision to publish the results.

References

1. Huang, P.; Kazlauciunas, A.; Menzel, R.; Lin, L. Determining the Mechanism and Efficiency of Industrial Dye Adsorption through Facile Structural Control of Organo-montmorillonite Adsorbents. *ACS Appl. Mater. Interfaces* **2017**, *9*, 26383–26391. [CrossRef]
2. Zhao, M.; Liu, P. Adsorption behavior of methylene blue on halloysite nanotubes. *Microporous Mesoporous Mater.* **2008**, *112*, 419–424. [CrossRef]
3. Weng, C.-H.; Pan, Y.-F. Adsorption of a cationic dye (methylene blue) onto spent activated clay. *J. Hazard. Mater.* **2007**, *144*, 355–362. [CrossRef]
4. Gong, J.L.; Wang, B.; Zeng, G.M.; Yang, C.P.; Niu, C.G.; Niu, Q.Y.; Zhou, W.J.; Liang, Y. Removal of cationic dyes from aqueous solution using magnetic multi-wall carbon nanotube nanocomposite as sorbent. *J. Hazard. Mater.* **2009**, *164*, 1517–1522. [CrossRef] [PubMed]
5. Fatimah, S.; Wang, D. Wulandari, ZnO/montmorillonite for photocatalytic and photochemical degradation of methylene blue. *Appl. Clay Sci.* **2011**, *53*, 553–560. [CrossRef]
6. Cottet, L.; Almeida, C.A.P.; Naidek, N.; Viante, M.F.; Lopes, M.C.; Debacher, N.A. Adsorption characteristics of montmorillonite clay modified with iron oxide with respect to methylene blue in aqueous media. *Appl. Clay Sci.* **2014**, *95*, 25–31. [CrossRef]
7. Peng, Y.G.; Chen, D.J.; Ji, J.L.; Kong, Y.; Wan, H.X.; Yao, C. Chitosan-modified palygorskite: Preparation, characterization and reactive dye removal. *Appl. Clay Sci.* **2013**, *74*, 81–86. [CrossRef]
8. Zhou, C.-H.; Zhang, D.; Tong, D.-S.; Wu, L.-M.; Yu, W.-H.; Ismadji, S. Paper-like composites of cellulose acetate–organo-montmorillonite for removal of hazardous anionic dye in water. *Chem. Eng. J.* **2012**, *209*, 223–234. [CrossRef]
9. Sivakumar, P.; Palanisamy, P.N. Adsorption studies of basic red 29 by a nonconventional activated carbon prepared from *Euphorbia antiquorum* L. *J. Chem. Tech. Res.* **2009**, *1*, 502–510.
10. Eren, E.; Afsin, B. Investigation of a basic dye adsorption from aqueous solution onto raw and pre-treated sepiolite surfaces. *Dyes Pigment.* **2007**, *73*, 162–167. [CrossRef]
11. Crini, G. Recent developments in polysaccharide-based materials used as adsorbents in wastewater treatment. *Prog. Polym. Sci.* **2005**, *30*, 38–70. [CrossRef]
12. Li, K.; Gao, Q.; Yadavalli, G.; Shen, X.; Lei, H.; Han, B.; Xia, K.; Zhou, C. Selective Adsorption of Gd3+ on a Magnetically Retrievable Imprinted Chitosan/Carbon Nanotube Composite with High Capacity. *ACS Appl. Mater. Interfaces* **2015**, *7*, 21047–21055. [CrossRef] [PubMed]
13. Lin, S.; Song, Z.; Che, G.; Ren, A.; Li, P.; Liu, C.; Zhang, J. Adsorption behavior of metal–organic frameworks for methylene blue from aqueous solution. *Microporous Mesoporous Mater.* **2014**, *193*, 27–34. [CrossRef]

14. Demey, H.; Tria, S.A.; Soleri, R.; Guiseppi-Elie, A.; Bazin, I. Sorption of his-tagged Protein G and Protein G onto chitosan/divalent metal ion sorbent used for detection of microcystin-LR. *Environ. Sci. Pollut. Res.* **2017**, *24*, 15–24. [CrossRef] [PubMed]
15. Demey, H.; Marchand, M.; Lapo, B.; Ruiz, M.; Fortuny, A.; Sastre, A. Neodymium Recovery by Chitosan/Iron(III) Hydroxide [ChiFer(III)] Sorbent Material: Batch and Column Systems. *Polymers* **2018**, *10*, 204. [CrossRef]
16. Awadh, S.M.; Abdulla, F.H. Purification of aqueous solutions from Pb (II) by natural bentonite: An empirical study on chemical adsorption. *Environ. Earth Sci.* **2017**, *76*, 386. [CrossRef]
17. Drweesh, S.A.; Fathy, N.A.; Wahba, M.A.; Hanna, A.A.; Akarish, A.I.; Elzahany, E.A.; El-Sherif, I.Y.; Abou-El-Sherbini, K.S.; Wahba, M.A. Equilibrium, kinetic and thermodynamic studies of Pb(II) adsorption from aqueous solutions on HCl-treated Egyptian kaolin. *J. Environ. Chem. Eng.* **2016**, *4*, 1674–1684. [CrossRef]
18. Deng, L.; Yuan, P.; Liu, D.; Annabi-Bergaya, F.; Zhou, J.; Chen, F.; Liu, Z. Effects of microstructure of clay minerals, montmorillonite, kaolinite and halloysite, on their benzene adsorption behaviors. *Appl. Clay Sci.* **2017**, *143*, 184–191. [CrossRef]
19. Belleville, P.; Popall, M.; Nicole, L.; Sanchez, C. Applications of advanced hybrid organic–inorganic nanomaterials: From laboratory to market. *Chem. Soc. Rev.* **2011**, *40*, 696.
20. Eugster, H.P. Hydrous sodium silicates from Lake Magadi, Kenya: Precurous of bedded chert. *Science* **1967**, *157*, 1177–1180. [CrossRef]
21. Thiesen, P.H.; Beneke, K.; Lagaly, G. Silylation of a crystalline silicic acid: An MAS NMR and porosity study. *J. Mater. Chem.* **2002**, *12*, 3010–3015. [CrossRef]
22. Wang, S.; Lin, M.; Shieh, Y.; Wang, Y.; Wang, S. Organic modification of synthesized clay-magadiite. *Ceram. Int.* **2007**, *33*, 681–685. [CrossRef]
23. Ge, M.; Zhu, C.; Wang, Y. Preparation and properties of organic quaternary phosphonium salts modified nano-magaiite/nylon6 composites. *Acta Mater. Compos. Sin.* **2017**, *34*, 33–52.
24. Ge, M.; Du, M.; Wang, Y. Adsorption Performance and Mechanism of Pb2+ on Mesoporous Material Magadiite. *J. Chin. Ceram. Soc.* **2017**, *45*, 37–45.
25. Attar, K.; Demey, H.; Bouazza, D.; Sastre, A.M. Sorption and Desorption Studies of Pb(II) and Ni(II) from Aqueous Solutions by a New Composite Based on Alginate and Magadiite Materials. *Polymers* **2019**, *11*, 340. [CrossRef]
26. Attar, K.; Bouazza, D.; Miloudi, H.; Tayeb, A.; Boos, A.; Sastre, A.M.; Demey, H. Cadmium removal by a low-cost magadiite-based material: Characterization and sorption applications. *J. Environ. Chem. Eng.* **2018**, *6*, 5351–5360. [CrossRef]
27. Joussein, E.; Petit, S.; Churchman, J. Halloysite clay minerals—A review. *Clay Miner.* **2005**, *40*, 383–426. [CrossRef]
28. Rawtani, D. Multifarious applications of halloysite nano tubes: A review. *Rev. Adv. Mater. Sci.* **2012**, *30*, 282–295.
29. Ouyang, J.; Zhou, Z.; Zhang, Y.; Yang, H. High morphological stability and structural transition of halloysite (Hunan, China) in heat treatment. *Appl. Clay Sci.* **2014**, *101*, 16–22. [CrossRef]
30. Barrientos-Ramírez, S.; Oca-Ramírez, G.M.; Ramos-Fernández, E.V.; Sepúlveda-Escribano, A.; Pastor-Blas, M.M.; González-Montiel, A. Surface modification of natural halloysite clay nanotubes with aminosilanes. Application as catalyst supports in the atom transfer radical polymerization of methyl methacrylate. *Appl. Catal. A Gen.* **2011**, *406*, 22–33. [CrossRef]
31. Wan, D.; Li, W.; Wang, G.; Chen, K.; Lu, L.; Hu, Q. Adsorption and heterogeneous degradation of rhodamine B on the surface of magnetic bentonite material. *Appl. Surf. Sci.* **2015**, *349*, 988–996. [CrossRef]
32. Xie, Y.; Qian, D.; Wu, D.; Ma, X. Magnetic halloysite nanotubes/iron oxide composites for the adsorption of dyes. *Chem. Eng. J.* **2011**, *168*, 959–963. [CrossRef]
33. Chang, J.; Ma, J.; Ma, Q.; Zhang, D.; Qiao, N.; Hu, M.; Ma, H. Adsorption of methylene blue onto Fe_3O_4/activated montmorillonite nanocomposite. *Appl. Clay Sci.* **2016**, *119*, 132–140. [CrossRef]
34. Kalantari, K.; Ahmad, M.B.; Masoumi, H.R.F.; Shameli, K.; Basri, M.; Khandanlou, R. Rapid and high capacity adsorption of heavy metals by Fe_3O_4/montmorillonite nanocomposite using response surface methodology: Preparation, characterization, optimization, equilibrium isotherms, and adsorption kinetics study. *J. Taiwan Inst. Chem. Eng.* **2015**, *49*, 192–198. [CrossRef]
35. Ge, M.; Chen, M. Preparation and characterization of magadiite. *J. Chin. Ceram Soc.* **2013**, *41*, 1704–1708.

36. Wang, X.; Wang, H.; Lu, M.; Teng, R.; Du, X. Facile synthesis of phenyl-modified magnetic graphene/mesoporous silica with hierarchical bridge-pore structure for efficient adsorption of pesticides. *Mater. Chem. Phys.* **2017**, *198*, 393–400. [CrossRef]
37. Meng, A.; Xiang, J.; Li, Z.; Li, Q. Cr-Doped ZnO Nanoparticles: Synthesis, Characterization, Adsorption Property, and Recyclability. *ACS Appl. Mater. Interfaces* **2015**, *7*, 27449–27457. [CrossRef]
38. Mall, I.D.; Srivastava, V.C.; Agarwal, N.K. Removal of Orange-G and Methyl Violet dyes by adsorption onto bagasse fly ash—Kinetic study and equilibrium isotherm analyses. *Dyes Pigment.* **2006**, *69*, 210–223. [CrossRef]
39. Almond, G.G.; Harris, R.K.; Franklin, K.R. A structural consideration of kanemite, octosilicate, magadiite and kenyaite. *J. Mater. Chem.* **1997**, *7*, 681–687. [CrossRef]
40. Xu, J.; Liu, X.; Lowry, G.V.; Cao, Z.; Zhao, H.; Zhou, J.L.; Xu, X. Dechlorination Mechanism of 2,4-Dichlorophenol by Magnetic MWCNTs Supported Pd/Fe Nanohybrids: Rapid Adsorption, Gradual Dechlorination, and Desorption of Phenol. *ACS Appl. Mater. Interfaces* **2016**, *8*, 7333–7342. [CrossRef] [PubMed]
41. Wang, C.; Feng, C.; Gao, Y.; Ma, X.; Wu, Q.; Wang, Z. Preparation of a graphene-based magnetic nanocomposite for the removal of an organic dye from aqueous solution. *Chem. Eng. J.* **2011**, *173*, 92–97. [CrossRef]
42. Guo, B.; Ouyang, J.; Yang, H. Adsorption Performance to Methylene Blue by Nano-Fe_3O_4 Assembled in Lumen of Halloysite Nanotubes. *J. Chin. Ceram Soc.* **2016**, *44*, 1655–1661.
43. Wang, Y.; Shang, Y.; Zhu, J.; Wu, J.; Ji, S.; Meng, C. Synthesis of magadiite using a natural diatomite material. *J. Chem. Technol. Biotechnol.* **2009**, *84*, 1894–1898. [CrossRef]
44. Zheng, P.; Du, Y.; Ma, X. Selective fabrication of iron oxide particles in halloysite lumen. *Mater. Chem. Phys.* **2015**, *151*, 14–17. [CrossRef]
45. Mu, B.; Wang, W.; Zhang, J.; Wang, A. Superparamagnetic sandwich structured silver/halloysite nanotubeFe_3O_4 nanocomposites for 4-nitrophenol reduction. *RSC Adv.* **2014**, *4*, 39439–39445. [CrossRef]
46. Rehman, M.A.; Yusoff, I.; Alias, Y. Fluoride adsorption by doped and un-doped magnetic ferrites $CuCe_xFe_{2-x}O_4$: Preparation, characterization, optimization and modeling for effectual remediation technologies. *J. Hazard. Mater.* **2015**, *299*, 316–324. [CrossRef]
47. Wang, W.; Feng, Q.; Dong, F.; Li, H.; Zhao, X. Preparation and properties of magnetic bentonite. *J. Chin. Ceram. Soc.* **2010**, *38*, 684–688.
48. Ge, M.; Cao, L.; Du, M.; Jahangir Alam, S.M. Adsorptive characterization of a pure magadiite and an organic modified magadiite on removal of methylene blue from related aqueous solution. *Mater. Chem. Phys.* **2018**, *217*, 533–540. [CrossRef]
49. Lou, Z.; Zhou, Z.; Zhang, W.; Zhang, X.; Hu, X.; Liu, P.; Zhang, H. Magnetized bentonite by Fe_3O_4 nanoparticles treated as adsorbent for methylene blue removal from aqueous solution: Synthesis, characterization, mechanism, kinetics and regeneration. *J. Taiwan Inst. Chem. E.* **2015**, *49*, 199–205. [CrossRef]
50. Ge, M.; Du, M.; Zheng, L.; Wang, B.; Zhou, X.; Jia, Z.; Hu, G.; Jahangir Alam, S.M. A maleic anhydride grafted sugarcane bagasse adsorbent and its performance on the removal of methylene blue from related wastewater. *Mater. Chem. Phys.* **2017**, *192*, 147–155. [CrossRef]
51. Ge, M.; Wang, X.; Du, M.; Liang, G.; Hu, G.; Jahangir Alam, S.M. Effects on the Mechanical Properties of Nacre-Like Bio-Hybrid Membranes with Inter-Penetrating Petal Structure Based on Magadiite. *Materials* **2019**, *12*, 173. [CrossRef]
52. Ge, M.; Wang, X.; Du, M.; Liang, G.; Hu, G.; Jahangir Alam, S.M. Adsorption Analyses of Phenol from Aqueous Solutions Using Magadiite Modified with Organo-Functional Groups: Kinetic and Equilibrium Studies. *Materials* **2019**, *12*, 96. [CrossRef]
53. Ge, M.; Cao, L.; Du, M.; Hu, G.; Alam, S.M.J. Competitive adsorption analyses of a pure magadiite and a New silylated magadiite on methylene blue and phenol from related aqueous Solution. *Mater. Chem. Phys.* **2018**, *217*, 393–402. [CrossRef]
54. Ge, M.; Du, M.; Zheng, L.; Zhou, X.; Jia, Z. Solid phase grafting preparation of SCB-g-MMA and its adsorption property. *Acta Mater. Compos. Sin.* **2016**, *33*, 2444–2453.
55. Shen, T.; Wang, Z.; Miao, W.; Zhou, Q.; Cheng, M.M.; Wang, Q.; Chen, Z.E. Study on adsorption of methylene blue on composite attapulgite material. *Dev. Appl. Mater.* **2009**, *24*, 44–48.

56. Huang, Z.; Li, Y.; Chen, W.; Shi, J.; Zhang, N.; Wang, X.; Li, Z.; Gao, L.; Zhang, Y. Modified bentonite adsorption of organic pollutants of dye wastewater. *Mater. Chem. Phys.* **2017**, *202*, 266–276. [CrossRef]
57. Tang, M.; Li, X.; Gao, C.; Li, X.; Qiu, H. Adsorption performance of CuFe2O4/rGO nanocomposites towards organic dye. *Mater. Chem. Phys.* **2017**, *185*, 114–121. [CrossRef]
58. Rehman, M.S.U.; Kim, I.; Han, J.I. Adsorption of methylene blue dye from aqueous solution by sugar extracted spent rice biomass. *Carbohydr. Polym.* **2012**, *90*, 1314–1322. [CrossRef]
59. Mokhtar, M.; Mostafa, M.M.M. Application of Synthetic Layered Sodium Silicate Magadiite Nanosheets for Environmental Remediation of Methylene Blue Dye in Water. *Materials* **2017**, *10*, 760. [CrossRef]
60. Li, C.; Zhong, H.; Wang, S.; Xue, J.; Zhang, Z. Removal of basic dye (methylene blue) from aqueous solution using zeolite synthesized from electrolytic manganese residue. *J. Ind. Eng. Chem.* **2015**, *23*, 344–352. [CrossRef]
61. Natarajan, T.S.; Bajaj, H.C.; Tayade, R.J. Preferential adsorption behavior of methylene blue dye onto surface hydroxyl group enriched TiO_2 nanotube and its photocatalytic regeneration. *J. Sci.* **2014**, *433*, 104–114.